Modeling and Analysis

Biofpr Biofuels Bioproducts & Biorefining

Ca-based bifunctional acid-basic model-catalysts for *n*-butanol production from ethanol condensation

Marina Pinzón, Marina Cortés-Reyes, Concepcion Herrera, Maria Á. Larrubia, Luis J. Alemany,
Departamento de Ingeniería Química, Facultad de Ciencias, Campus de Teatinos, Universidad de Málaga, Málaga, Spain

Received June 08 2020; Revised August 18 2020; Accepted September 01 2020;
View online at Wiley Online Library (wileyonlinelibrary.com);
DOI: 10.1002/bbb.2155; *Biofuels, Bioprod. Bioref*. (2020)

Abstract: Ethanol to *n*-butanol conversion is a process that can increase the carbon number of alcohols by coupling. There is increasing interest in the mechanisms for *n*-butanol production in a simple step through the effective use of bifunctional acid–base catalysts. In this context, commercial hydroxyapatite (HAP) and two synthetized model supported catalysts, Ca/Al_2O_3 and $Ca\text{-}P/Al_2O_3$, were used in bioethanol condensation. Characterization and acid–base sites were considered, and Fourier-transform infrared (FTIR) spectroscopy and diffuse reflectance infrared Fourier-transform spectroscopy–mass spectrometry (DRIFT-MS) reactivity tests were performed *in situ*, as a first approximation to design a sustainable catalytic process rationally, and with the aim of understanding the process at the catalytic surface. The results indicated that the reactions occur at a large range of temperatures (200–450 °C). Hydroxyapatite and Ca/Al_2O_3 have similar basic sites (low and medium) and $Ca\text{-}P/Al_2O_3$ presented the strongest Brönsted and Lewis combined acid sites. Three major reactions were identified: non-oxidative dehydrogenation, aldol condensation, and intermolecular reduction, associated with the basic-acid sites Ca-O-Ca/Ca-O-P/Ca-O-Al. Side reactions also occur involving different acid sites related to Lewis alumina centers favoring ethylene or diethyl-ether production.

Keywords: acid–base catalysts; bioethanol; *n*-butanol; condensation

Introduction

In the field of biofuels, alcohols have been used primarily in spark ignition engines. Ethanol produced from biomass is blended in low concentrations into gasoline and is also sold in high-concentration blends for flexible fuel vehicles. Ethanol and two isomers of butanol, *n*-butanol and isobutanol, can be produced from biomass at a cost and with energy inputs that are relatively comparable with those of diesel fuel. In general, they have lower viscosity, higher volatility, and lower cetane numbers (ethanol 5–8 and *n*-butanol 17–25) than diesel fuel. Ethanol and *n*-butanol have also been considered for use in diesel engines, with *n*-butanol being more suitable than ethanol due to its higher density, viscosity, lubricity, and cetane number. Butanol is also miscible with diesel fuel without additional co-solvents.[1,2]

Several investigations have shown that *n*-butanol can be produced by a catalytic route from ethanol. This involves a cross-coupling between alcohols, promoted by homogeneous or heterogeneous catalysts.[3–5] These processes

Correspondence to: Luis J Alemany or Concepcion Herrera, Departamento de Ingeniería Química, Facultad de Ciencias, Campus de Teatinos, Universidad de Málaga, Málaga, E-29071, Spain. E-mail: luijo@uma.es (Alemany), E-mail: concepcionhd@uma.es (Herrera)

are considered to be economical and green.[6] However, the best results have been obtained using heterogeneous catalysts because the homogeneous catalysts produce long chain alcohols (>4 carbon).[7] Different heterogeneous catalysts have been studied for this purpose, such as zeolites, basic metal oxides such as MgO, Mg-Al mixed oxides, metal oxides with different metal loadings, and bifunctional catalysts.[6,8–12]

In particular, zeolites require high reaction temperatures to produce butanol. Yang and Meng[13] investigated the incorporation of metals such as Rb and Li with zeolites to improve the yields. Basic metal oxides catalysts such as MgO have been considered good catalysts in ethanol coupling to *n*-butanol and 1,3-butadiene; however, the reaction demands a higher temperature (>400 °C) and acetaldehyde production inhibits the formation of C-C bonds and causes deactivation of MgO catalysts.[5,14,15] Moreover, mixed oxides obtained from hydrotalcites have been studied to increase the activity of MgO because of their suitable acid–base pairs. León *et al.*[16] compared Mg-Al and Mg-Fe catalysts in this reaction. In this context, when Al^{3+} is exchanged by Fe^{3+}, the acid sites decrease in the catalyst increasing the selectivity to acetaldehyde and higher alcohols. The addition of noble metals (Ru, Pd or Cu) to mixed oxides increases *n*-butanol selectivity; on the other hand, Mg-Zr mixed oxides are poisoned by acetaldehyde species during ethanol condensation.[10,17,18]

Currently, metal oxides catalysts are used commercially due to their acid–base properties. Riittonen *et al.*,[19] studied alumina catalysts modified with different metals (Co, Ni, Cu, Ru, Pd, Pt, and Ag) to produce *n*-butanol but the reaction was found to be very sensitive to metal loading. They proposed that the structure of Ni- and Cu- over alumina catalysts have active sites for this reaction.[20]

On the other hand, there is strong interest in the use of bifunctional catalysts like hydroxyapatite (HAP) ($Ca_5(PO_4)_3OH$).[21–26] This mineral is very stable, due to its crystallinity, and has a good affinity for organic compounds. The acid–base properties of these materials can be modified due to the Ca/P ratio, and the yields of ethanol condensation present better results when Ca/P is between 1.5 and 1.67.[27,28] Different authors have synthesized strontium hydroxyapatite, because acid and basic sites increase with increasing strontium loading, improving the *n*-butanol selectivity.[29,30]

Some authors emphasize that it is a crucial factor for the development of a selective catalyst to balance the acid and basic sites of catalyst correctly because the strongly acidic sites cause the molecular dehydration of ethanol, producing ethylene and ethers, including decomposition of ethanol in gaseous products (CO, CH_4, CO_2, and H_2).[31,32] Although the condensation of alcohols has been investigated with different catalysts, the mechanism and operating conditions have not yet been clearly defined.

The most commonly accepted catalytic process for the transformation of ethanol to *n*-butanol is known as the Guerbet reaction. This consists of four steps, including a first dehydrogenation of ethanol to form acetaldehyde, followed by an aldol condensation of two molecules of acetaldehyde, a later dehydration of the aldol product, and a final hydrogenation to form butanol; this is considered an indirect route.[26,27,33] Another mechanism has been proposed by other authors and is known as a direct route.[23,28,34,35] The direct route requires high temperatures; this mechanism consists of the direct coupling of two alcohol molecules with water production. Scalbert *et al.*[23] proposed another mechanism based on the condensation of a molecule of ethanol and a molecule of aldehyde.

In the present contribution, a commercial HAP and two model alumina supported Ca-containing catalysts, Ca/Al_2O_3 and $Ca\text{-}P/Al_2O_3$, prepared in our laboratory, were characterized and tested in the gas-phase ethanol condensation reaction. The distribution of acid and basic sites was studied and reactivity tests were performed by spectroscopic techniques and under working conditions to gain some insight into the species present or interacting with the catalytic surface related to the acid/base pairs and the reaction route.

Experimental

Catalyst preparation

Two model catalysts were synthesized by the incipient wetness impregnation of commercial alumina (γ-Al_2O_3-TH Sasol Puralox, 150 $m^2\ g^{-1}$), a common technique for the synthesis of heterogeneous catalysts. The method was adapted to our system and the synthesis was approached in two steps. First, Ca/Al_2O_3 catalyst was obtained after impregnation of the γ-Al_2O_3 support with an aqueous solution of calcium acetate ($Ca(CH_3COO)_2$, 99% Fluka) with a metal loading of 4 at·nm^{-2}, then, it was dried overnight at 353 K and calcined in two steps (1 h at 623 K and 2 h at 773 K) in air. $Ca\text{-}P/Al_2O_3$ catalyst was then obtained after impregnation of Ca/Al_2O_3 with an aqueous solution of phosphoric acid (H_3PO_4, 85% Panreac) prepared to obtain a Ca/P atomic relation of 1.5, then it was dried overnight at 353 K and calcined for 2 h at 598 K and for 3 h at 773 K in air. Commercial HAP, $Ca_{10}(PO_4)_6(OH)_2$ (Across Organics), was calcinated for 2 h at 873 K.

 | *Biofuels, Bioprod. Bioref.* (2020); DOI: 10.1002/bbb.2155

Catalyst characterization

Morphological and textural parameters (A_{BET}, V_p and pore size) were determined using the Brunauer–Emmet–Teller (BET) method on a Micromeritics ASAP 2020 analyzer from nitrogen adsorption isotherms. X-ray diffraction (XRD) patterns were recorded using an X'Pert MPD Pro diffractometer (PANanalytical) equipped with Cu K-α monochromated radiation, and the diffractograms were collected in the 2θ angle range between 10° and 70°. X-ray photoelectron spectroscopy (XPS) was performed using a Physical Electronics 5701 spectrometer equipped with a PHI 10–360 analyzer, with a Mg Kα X-ray source. All the binding energy (BE) values given were referred to the C1s signal (284.8 eV) from the adventitious carbon. Deconvolution of experimental curves was done with Gaussian and Lorentzian line fitting, minimizing the χ^2 values.

Ammonia temperature-programmed desorption (NH_3-TPD) experiments were carried out in a flow system using 100 mL·min^{-1} of gas with 1000 ppm of NH_3 and a temperature ranging from 323 to 923 K with a ramp of 10 K·min^{-1} in helium. The sample, 60 mg of catalyst, was placed in a quartz U-shaped reactor and was cleaned for 1 h at 773 K in helium. Ammonia was then adsorbed at 323 K, a helium purge was performed, and finally the temperature was increased. The outlet gases were analyzed with a QMS 200 mass spectrometer (Pfeiffer Vacuum Prisma™).

A procedure similar to the one described for NH_3-TPD was employed in the case of carbon dioxide temperature-programmed desorption (CO_2-TPD). The sample was cleaned in He at 773 K for an hour. The experiments were carried out using 100 mL·min^{-1} flow with 1000 ppm of CO_2 and a temperature range from 323 to 923 K with a ramp of 10 K·min^{-1} in helium.

Catalytic activity

Fourier-transform infrared spectra were obtained from a self-supported disk placed in a quartz cell equipped with KBr windows and connected to a vacuum line allowing thermal treatments and adsorption–desorption experiments to be carried out *in situ* using a Nicolet Nexus 6700 FTIR spectrometer. Samples were first heated at 923 K in vacuum for 2 h (named as activated catalysts) and pulses of ethanol (5 Torr) were introduced at 323 K. The surface spectra were obtained from 323 to 773 K in gas evacuation. Anhydrous ethanol (99.9% Panreac) was used in all experiments. The spectra shown are subtraction spectra, in which, each spectrum is the result of the subtraction of the spectrum after ethanol admission and the one of the activated catalyst.

An *in situ* diffuse reflectance infrared Fourier-transform – mass spectrometry (DRIFT–MS) study of ethanol temperature-programmed reaction was carried out in a continuous flow Harrick Praying Mantis™ reaction chamber equipped with ZnSe windows and connected to the QMS 200 mass spectrometer. The experiments were collected at atmospheric pressure in the FTIR Nicolet Nexus 6700 spectrometer, whereas outlet gas was analyzed by mass spectrometry (MS). First, the surface of the catalysts was cleaned at 773 K in a He flow (25 mL·min^{-1}) for 1 h and was cooled. These spectra were taken as references prior to ethanol admission to the cell. The saturation of ethanol was carried out at 323 K with 1.4 mL·min^{-1} ethanol flow and a Gas Hourly Speed Velocity (GHSV) of 1.8·10^4 h^{-1}. After saturation was achieved, a purge of He was performed to eliminate the remaining ethanol. Desorption of ethanol was conducted under a helium flow at temperatures between 323 and 773 K at a rate of 10 K·min^{-1}. Different m/z fragments were monitored to identify ethanol, *n*-butanol, ethylene, diethyl ether, and acetaldehyde.

Results and discussion

Catalysts characterization

The diffraction patterns of the calcined catalysts are displayed in Fig. 1. The XRD patterns for HAP show that this catalyst is mainly composed of crystalline hydroxyapatite, with the main lattice structure being $Ca_5(PO_4)_3OH$, (JCPDS 05-0656).[27] The characteristic structure for the support, γ-alumina poorly crystalized (JCPDS 75-0921), was observed for all the synthesized materials. Moreover, Ca/Al_2O_3 presented signals

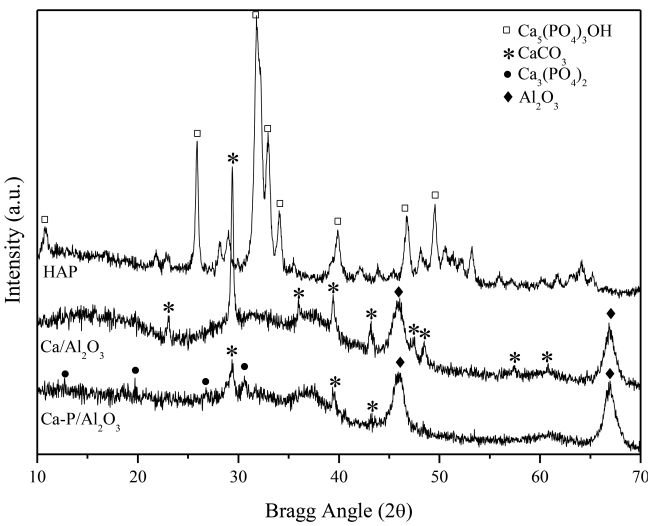

Figure 1. XRD pattern of the calcined catalysts.

at 29, 39, and 43° (2θ) associated with calcium carbonate ($CaCO_3$)[36] and the Ca-P/Al_2O_3 also exhibited signals related to $Ca_3(PO_4)_2$ (JCPDS 09-0348).

The textural properties of, and XPS data for, the alumina support, model catalysts (Ca/Al_2O_3 and Ca-P/Al_2O_3) and HAP are summarized in Table 1. The alumina used as support presents the highest surface area and pore volume with values of 166 $m^2 \cdot g^{-1}$ and 1.19 $cm^3 \cdot g^{-1}$, respectively. The impregnation of the support with 4 at of $Ca \cdot nm^{-2}$ for Ca/Al_2O_3 catalyst, which can represent a theoretical surface coverage close to 60%, results in a decrease in the BET surface area and pore volume, with values of 114 $m^2 \cdot g^{-1}$ and 0.42 $cm^3 \cdot g^{-1}$, respectively. For Ca-P/Al_2O_3 catalyst, with a Ca/P atomic ratio = 1.5, the diminution of the BET surface is close to half; meanwhile, the pore volume and the pore size presented for the supported catalyst are quite similar. The A_{BET} and V_p for HAP, (Ca/P atomic ratio = 1.67) were 41 $m^2 \cdot g^{-1}$ and 0.34 $cm^3 \cdot g^{-1}$, respectively. As was expected, the decrease in the A_{BET} of the alumina supported catalyst was a consequence of the coverage by the incorporation of Ca and P into the support.

The Ca/Al ratios registered by XPS (Table 1) presented very different values for the alumina supported samples. So, for Ca/Al_2O_3, the Ca/Al ratio is very low (0.05) and lower than the theoretical ratio taking into aacount that according to the preparation procedure, it was incorporated 4 atoms of Ca pero nm^2 of alumina support. The Ca/Al ratio registered for Ca-P/Al_2O_3 (0.24) is also five times higher than that used in the preparation due to the fact that the addition of phosphoric acid causes the formation of $Ca_3(PO_4)_2$ and the Ca-bonded phosphorous species spread leaving part of alumina surface uncovered. There is also segregation of some of the calcium ions that form calcium carbonate on the catalyst's surface, which also subtracts Ca interacting directly with the alumina. The Ca/P ratio for HAP determined by XPS was 1.52, somewhat less than the theoretical atomic ratio, whereas for the Ca-P/Al_2O_3 catalyst it was 0.62, three times lower than that used in the preparation, related to the different atomic distributions by different crystalline species formation (P/Al = 0.03) during the synthesis procedure and the surface dispersion capacity of the alumina support.

The BE values and percentage distribution data of species, from Ca 2p3/2 and P 2p deconvoluted XPS-signals are displayed in Table 1. For HAP, the Ca2p3/2 and P2p symmetrical bands showed maximums at 346.9 eV. and 132.8 eV., respectively, which correspond to hydroxyapatite $Ca_{10}(PO_4)_6(OH)_2$, in which the crystalline unit is contribution by two entities.[37] For Ca/Al_2O_3 model catalyst, a non-symmetrical calcium-signal was detected with a BE maximum value at 347.7 eV, which was correlated with the presence of partially carbonated calcium oxide. For Ca-P/Al_2O_3, the asymmetry of the Ca-band increases, and at least two contributions are denoted with maxima observed at 346.8 and 347.7 eV. that are associated with $CaO/CaCO_3$ and $Ca_3(PO_4)_2$, respectively, in agreement with the phases detected by XRD. Only a single symmetric signal was recorded for phosphorous in the P2p region, with a maximum at 133.8 eV, which is related to $Ca_3(PO_4)_2$ formation.[38]

The acid–base properties of the catalysts, in terms of strength and number of sites, were determined using NH_3-TPD and CO_2-TPD, and desorption profiles are represented in Figs 2 and 3, respectively. The NH_3 profiles during a temperature ramp at 10 $K \cdot min^{-1}$ are displayed in Fig. 2 together with the deconvolution of the curves for the catalysts, carried out using the Gaussian method. Hydroxyapatite showed a wide desorption band between 323 K and 645 K that can be deconvoluted in two main contributions; the first one between 323 and 473 K related to weak acid sites and the second between 430 and 645 K associated with medium-strength sites. Silvester *et al.*[39] have reported that the acidity of HAP materials depends on certain surface properties such as the Ca/P ratio or crystal size. For the HAP used in this study, the Ca/P molar ratio is 1.52 and weak and medium-strength acid sites were found. The acidic properties of hydroxyapatites were attributed to surface HPO_4^{2-} and OH^- vacancies mainly occurring on Ca-deficient samples, and higher Ca content in samples is expected to

Table 1. Summary of textural properties and XPS data.

Materials	A_{BET} (m^2 g^{-1})	Pore volume (cm^3 g^{-1})	Pore size (Å)	XPS data			
				Ca2p3/2*	P2p**	Ca/P ratio	Ca/Al ratio
Al_2O_3 (TH)	166	1.19	288	—	—	—	—
Ca/Al_2O_3	114	0.42	145	347.4 (100)	—	—	0.05
Ca-P/Al_2O_3	88	0.31	141	346.8 (42) 347.7 (58)	133.8 (100)	0.62	0.24
HAP	41	0.34	324	346.9 (100)	132.8 (100)	1.52	—

*relative Ca population from Ca2p3/2 deconvolution.
**relative P population from P2p deconvolution.

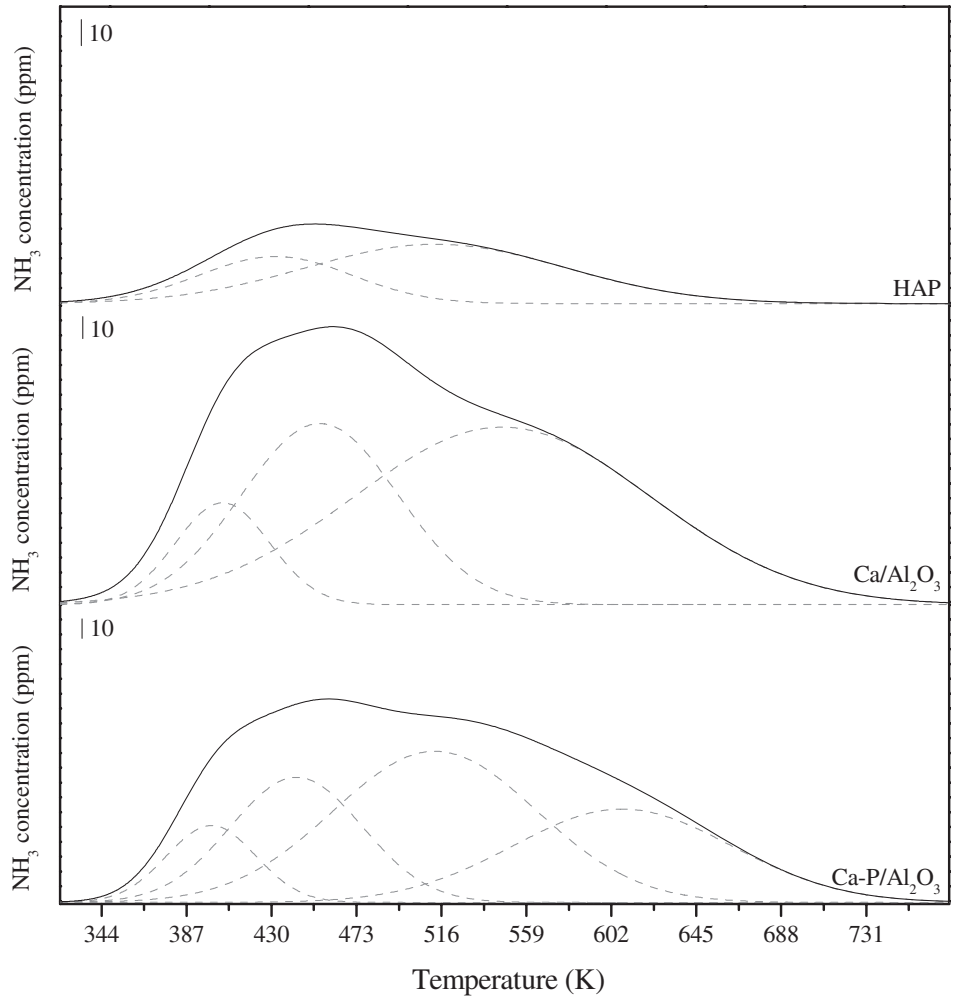

Figure 2. NH_3-TPD profiles of the catalysts in helium from 323 to 923 K at 10 K·min^{-1}.

decrease the number of acid sites due to the formation of CaO species on the hydroxyapatite surface. In the desorption of NH_3 for the Ca/Al_2O_3 catalyst, three bands were detected at 345–420 K, 385–560 K, and 430–773 K, and are related to weak, medium, and strong acid sites, respectively, and an only slight decrease in the total acidity of the alumina was denoted[40] (data not showed for brevity). This behavior must be attributed to the exposed alumina because the Ca/Al ratio is very low (0.05). On the other hand, the deconvolution of the curve of $Ca\text{-}P/Al_2O_3$ shows at least four peaks between 344 K and 730 K. The broad desorption band of this catalyst is associated with the high ammonia adsorption capacity and the number of Brönsted and Lewis acid sites, showing stronger acid sites than the other catalysts; this behavior can be in part associated with the acid character of the alumina support and the presence of Lewis Al^{3+} sites (Ca/Al ratio is 0.26, what implies almost 75% of exposed alumina) and promoted by the acid character of phosphorus. Moreover,

Table 2. Net adsorption capacity of probe molecules.

Sample	HAP	Ca/Al_2O_3	$Ca\text{-}P/Al_2O_3$
$mmol NH_3 \cdot g_{cat}^{-1}$	0.29	0.40	0.42
$mmol CO_2 \cdot g_{cat}^{-1}$	0.13	0.06	0.02

the net ammonia adsorption capacity for the systems was estimated from the isothermal adsorption curve at 323 K and the values are presented in Table 2. Hydroxyapatite is the least acidic material, with an almost 30% lower ammonia adsorption capacity and the alumina based- synthesized materials showed similar ammonia adsorption capacity (0.40–0.42 mmol $NH_3 \cdot g_{cat}^{-1}$) with a slight increase due to the incorporation of phosphorous to the formulation.

The profiles and deconvolution of CO_2-TPD for the samples are shown in Fig. 3. The deconvolution shows two dominant bands between 323 K and 688 K related to different basic

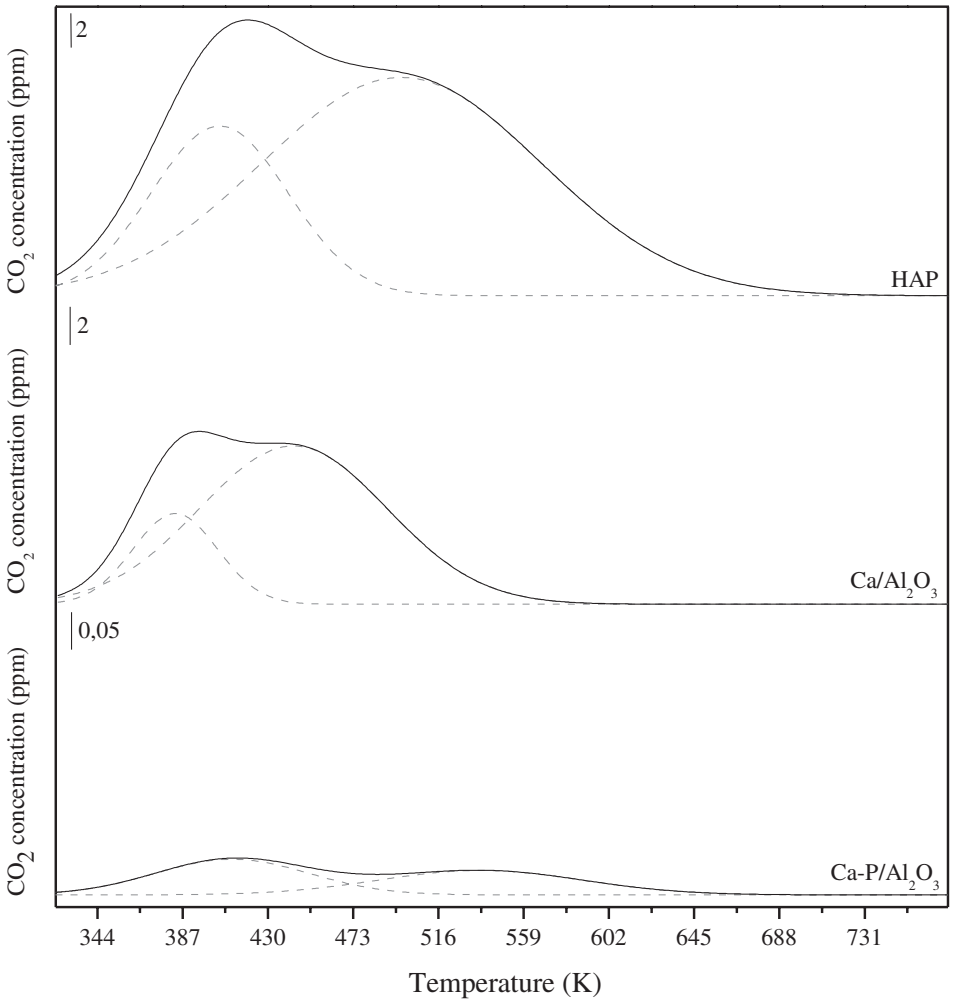

Figure 3. CO_2-TPD profiles of the catalysts in helium from 323 to 923 K at 10 K·min^{-1}.

strengths. For HAP, the first band (323–473 K) is associated with medium basic sites and the second peak (473–688 K) is attributed to medium-strong basic sites, in line with O^{2-} and OH^- presence and accessible Ca^{2+} sites. Some authors[41] have identified the presence of two basic sites (OH^- and O^{2-}) when CO_2 is adsorbed over HAP, using spectroscopic analytical techniques, and other authors suggested that O^{2-} sites are less basic than OH^- sites.[22] Tsuchida *et al.*[27] related the basic HAP sites to the existence of Ca^{2+} ions. For Ca/Al_2O_3 catalyst, two peaks can be distinguished – the first corresponds with medium-weak basic sites and the second peak, between 400 and 585 K, is associated with medium Lewis sites of the type Ca-O and Al-O,[42] with a CO_2 adsorption value of 0.06 mmol·g_{cat}^{-1}, which is half of that obtained for HAP. Liu *et al.*[36] also affirmed the presence of Ca-O-Al sites due to a desorption peak of CO_2 at 821 K, and other authors[43] related the lower basicity of CaO-Al catalyst to the presence of carbonates species over the surface. Finally, the Ca-P/Al_2O_3 catalyst shows the lowest adsorption of CO_2, retaining 0.02 mmol of CO_2 per gram of catalyst and two small bands can be envisaged, with a profile quite similar to that described for HAP.

The acid–base data of the catalysts showed that HAP and Ca/Al_2O_3 have similar basic sites. However, the Ca-P/Al_2O_3 catalyst has the highest strength acid sites, associated with the contribution of the exposed alumina support and its modification with the addition of P-atoms as some authors indicated.[44]

Catalytic reaction

The infrared spectra registered after the adsorption of 5 Torr of ethanol were followed by thermal desorption at increasing temperatures, and are displayed for the activated catalysts in Fig. 4 to identify the species present in the catalytic surface. For HAP, the initial spectrum after vacuum treatment at 323 K (spectrum a) presented bands in the C-H stretching

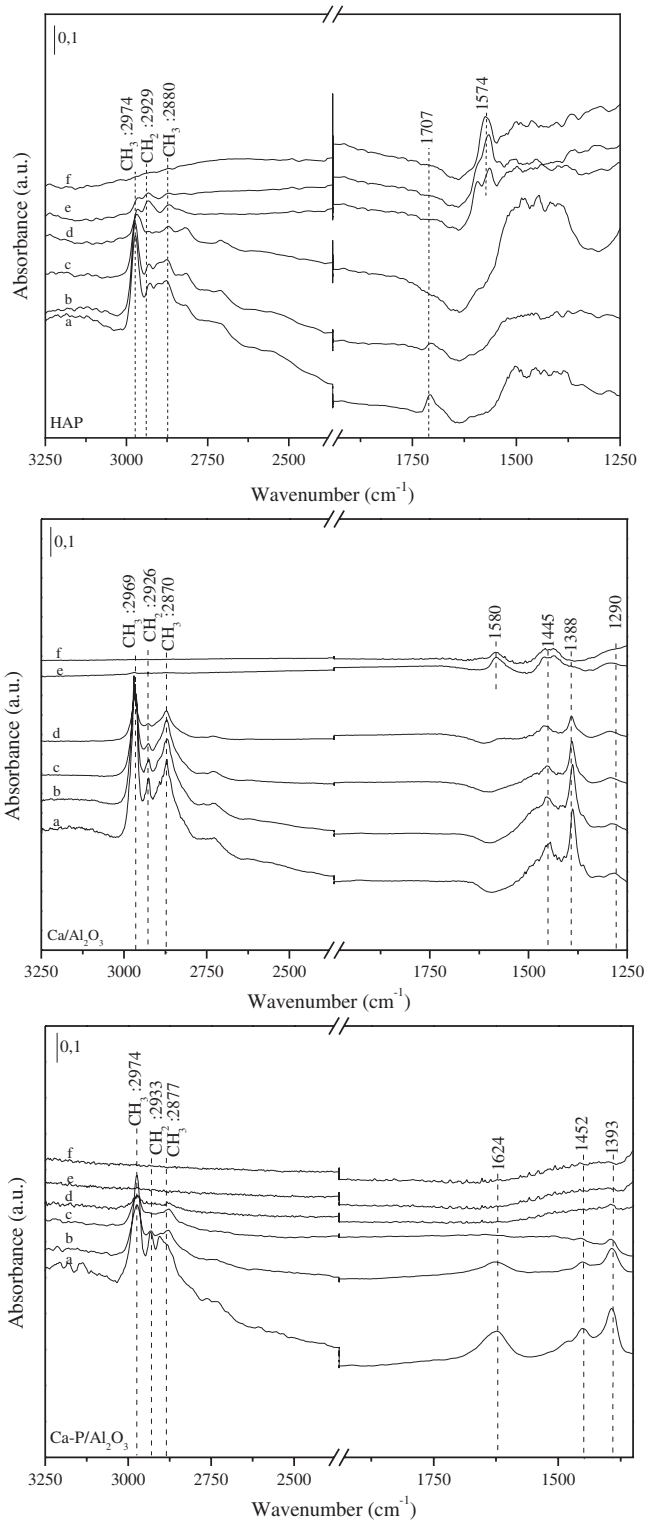

Figure 4. FTIR spectra of ethanol adsorbed on the catalysts after evacuation at (a) 323 K, (b) 373 K, (c) 473 K, (d) 573 K, (e) 673 K and (f) 773 K.

region (3100–2600 cm^{-1}) whose intensities decrease with the increase in the temperature. The signal that appears at 1707 cm^{-1}, related to the C=O stretching mode of the acetaldehyde surface species formed, is also observable at lower temperatures.[45] On the spectra, poorly resolved bands associated with ethoxide-surface species between 1500 and 1390 cm^{-1}[24,46] were registered and superimposed on molecularly adsorbed ethanol bands, where a very weak signal at 1276 cm^{-1} that remained to 473 K was observed. Upon thermal outgassing, the progressive disappearance of the bands is observed and at 573 K as evacuation temperature a signal at 1574 cm^{-1} stands out, mainly associated with the acetate species formation. Carvalho *et al.*[47] indicated that the presence of surface acetate species is the result of formation of acetaldehyde by a surface condensation reaction. Other authors reported that at low temperatures only ethanol is retained, and the formation of acetate species is not observed. Likewise, the same authors[48] by DRIFT experiments with HAP registered the presence of a signal at 1568 cm^{-1} related to these acetate-species but at higher temperatures. In this case, the formation of acetaldehyde-acetate species was observed at both low and high temperatures, which suggests different bonds on the HAP-surface.

Regarding the spectra obtained for Ca/Al_2O_3 after adsorption of ethanol and their evolution with temperature, it can be observed that this catalyst presents certain differences compared with HAP as reference. Bands between 1450–1390 cm^{-1}, especially at the lower evacuation temperatures, are well resolved and related to ethoxy and ethyl-acetate species. After 573 K, weak signals arise at 1445 and 1580 cm^{-1} related to remaining ethoxy and acetate/carboxylate species when ethanol on the surface completely disappears.[49] Alumina was used as a support for Ca/Al_2O_3 and $Ca\text{-}P/Al_2O_3$ catalysts and to evaluate the contribution of the exposed alumina, ethanol adsorption and evacuation in temperature have been verified. The interaction of alumina with ethanol occurs through the pair of electrons of EtOH, involved to form mainly ethoxy species which decompose to form ethylene; besides, the cleavage of hydroxyl groups of ethanol would result in acetate/carboxylate species formation than can also react with the temperature persistent ethoxy-groups, derived from dissociative chemisorption onto alumina. In line with an earlier reported study,[47] the dehydrogenation and condensation reactions do not occur on the alumina used as support, and the main product observed for ethanol transformation onto alumina was ethylene.

The infrared (IR) response for ethanol adsorption on $Ca\text{-}P/Al_2O_3$ is also different because of the incorporation of P in the formulation. As can been observed at 373 K, there are clear additional bands at 1624, 1452, and 1393 cm^{-1} due

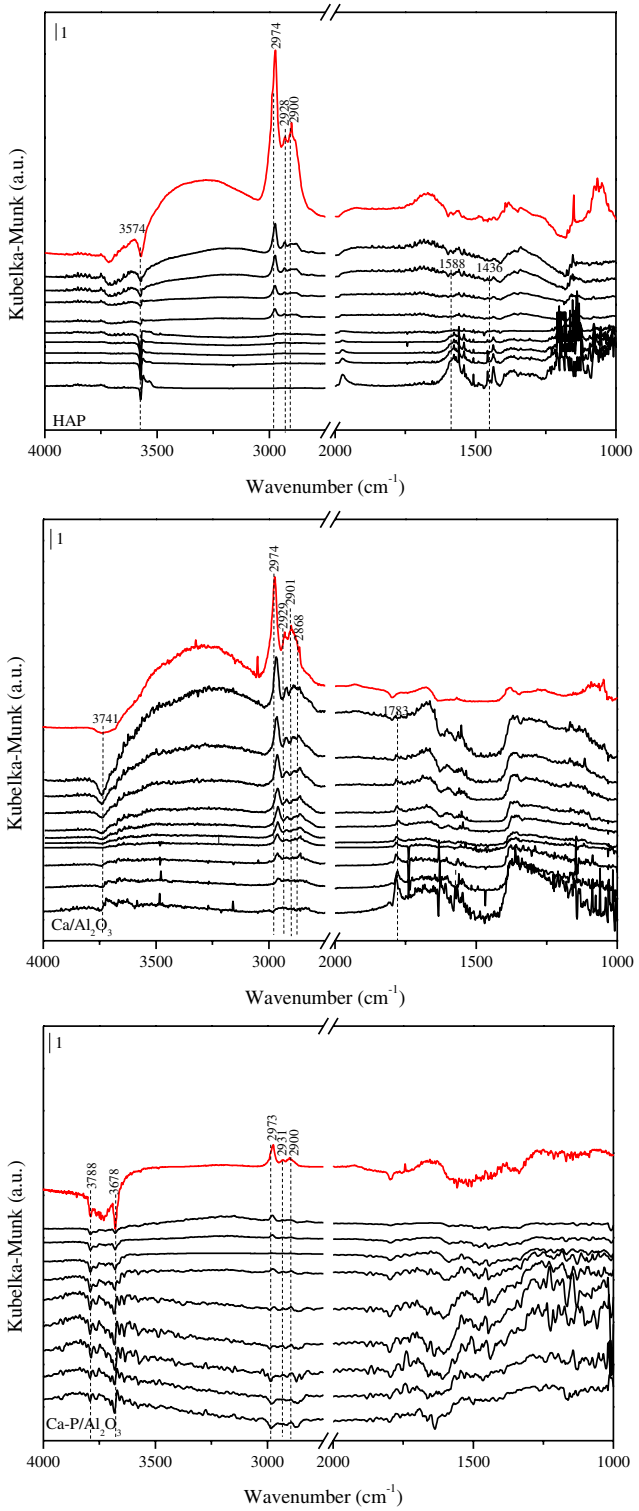

Figure 5. DRIFT spectra of ethanol saturation at room temperature (red lines) and desorption of ethanol in helium (black lines) in descent order of 50° from 323 to 673 K.

to the formation of water, ethyl-acetate, and the ethoxy species, respectively. They are removed at 473 K. The broad and relatively weak band centered at 1624 cm^{-1} detected after outgassing at room temperature and 323 K could be associated with water strongly bonded to phosphoric groups and water-formation by side condensation reactions. The presence of signals related to ethyl-acetate and ethoxy species disappeared after outgassing at 473 K, a lower temperature than those observed for free-P catalyst, Ca/Al_2O_3 Acetaldehyde/carboxylate bands weren't detected. These observations indicated a weaker interaction of ethanol with catalyst's surface and due to the combination of the acidity properties and the alumina exposed surface, the promotion of both the condensation reaction to form spectator-species retained on surface and, according to the data reported by Phung and Busca,[50] and the dehydration routes to form ethylene and diethyl ether (DEE) at lower temperatures.

Figure 5 shows the DRIFT spectra of ethanol saturation over different catalysts at 323 K (red lines) and the desorption of ethanol in helium (black lines) from 323 K to 773 K, withspectra taken every 50° and represented in descending order in the figure. Hydroxyapatite, Ca/Al_2O_3 and, to a lesser extent, $Ca\text{-}P/Al_2O_3$ catalysts, showed peaks related to methyl groups ($CH_3\nu$, $CH_2\nu$ and $CH_3\nu$) of ethoxide species ($CH_3CH_2O^-$) over the surface. A typical spectrum collected after an ethanol pulse at 323 K displayed three/four peaks in the region between 2980 and 2850 cm^{-1}. Vibrations close to 2972 and 2928 cm^{-1} have been attributed to the CH_3 group and the modes at 2892 and 2872 cm^{-1} vibrations were associated with CH_2 groups in monodentate species (CH_3CH_2O-M) and bidentate ethoxy species coordinated to two metal atoms (CH_3CH_2O-M-M), respectively, where M represents the alkaline-metal.[51,52] Both the intensity and the modes in the recorded spectra are slightly shifted for the different catalysts and the way in which ethanol molecule is able to interact with the catalytic surface is decisive in directing the distribution of products towards one or another compound. The intensity and the strength of adsorbed species at higher (bidentate) and lower (monodentate) wavenumbers also represent the balance ethoxy-groups species and its surface coverage. So, both monodentate and bidentate ethoxy-species are common and visible independently of the surface nature and the initial reaction products detected. HAP catalyst mainly showed modes related to monoethoxy groups, which are maintained until temperatures close to 473 K are reached. For Ca/Al_2O_3 catalyst, the major monodentate ethoxy-species are also evidenced and remain visible up to temperatures close to 573 K i.e., 100° above. For $Ca\text{-}P/Al_2O_3$ catalyst, the signals are mainly associated with a lower population of monodentate species but disappear at

temperatures higher than 423 K. Except for HAP catalyst, the presence of bidentate ethoxy-groups is discarded, although the population of these species is apparently lower than monodentate species.

The desorption at higher temperatures over HAP showed bands at 1588 and 1435 cm^{-1}, which were associated with strongly bounded acetate species that came from adsorbed acetaldehyde. In contrast, the desorption of ethanol at higher temperature over Ca/Al_2O_3 showed a signal at 1783 cm^{-1} related to acetaldehyde species. $Ca\text{-}P/Al_2O_3$ catalyst presents very different behavior because, in the DRIFT spectra, other signals are not distinguished on the catalyst surface.

The product distribution in the gas-off stream of DRIFT-MS experiments from the saturation and temperature desorption of ethanol are represented in Fig. 6. Acetaldehyde, DEE, ethylene and *n*-butanol were major products detected. In the panel corresponding to acetaldehyde evolution with temperature, expressed as relative intensity of m/z normalized signal, for HAP it is possible to detect a broad and extended band between 323 and 700 K, with a relative maximum at 522 K (black line). However, acetaldehyde formation over Ca/Al_2O_3, showed two maxima with a similar contribution localized at 428 and 634 K (red line) coming from two different

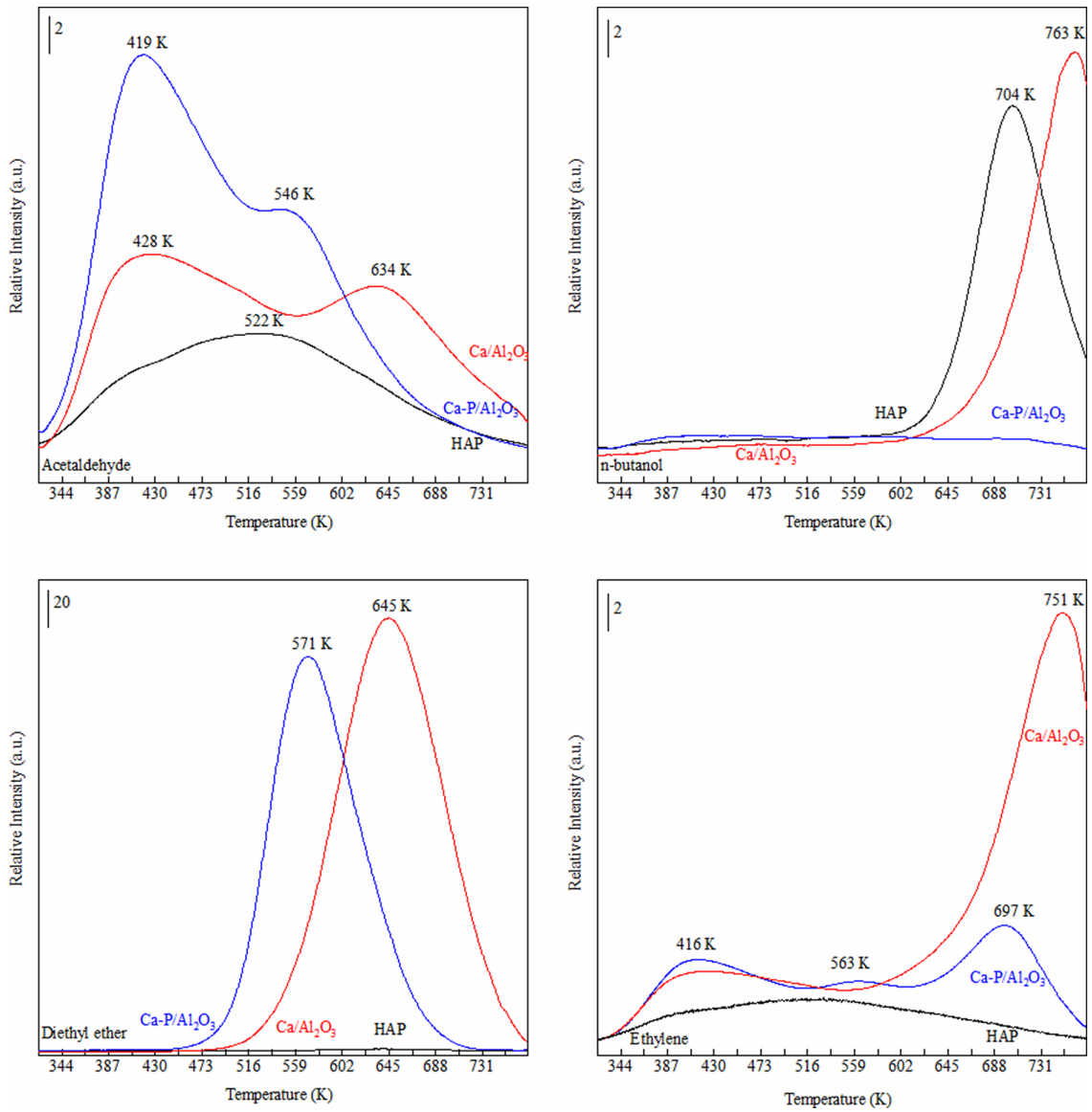

Figure 6. Acetaldehyde, *n*-butanol, diethyl ether and ethylene production over the catalysts as a function of temperature during ethanol desorption in DRIFT-MS experiments.

processes that involved multifunctional centers. For Ca-P/Al_2O_3 catalyst those maxima were also registered, but at a lower temperature with respect to P-free Ca-Al_2O_3 catalyst, at 419 K and 546 K (blue line), while the relative contribution is higher at lower temperature which in part should be associated with similar sites but with stronger acid-basic properties. Acetaldehyde is formed through the transformation of a single ethoxide-species; however, the formation of condensed and dehydrogenated products required the interaction of multiple ethoxide species on the surface. So, the primary production of acetaldehyde is related to the route of ethanol dehydrogenation over strong or medium basic sites, in particular, Ca-O-Ca or even Ca-O-Al type sites, for these catalysts.[17,23,42,44,45] Besides, another route can be attributed to the dissociative adsorption of ethanol to form a monoethoxide groups on Lewis acid sites and the subsequent dissociation into acetaldehyde.

From a catalytic standpoint, it is thought that active sites on the surface of HAP and those of the alumina-supported Ca containing and P sites with different Ca/P and Ca/Al molar ratios, could explain the peculiar distribution of reaction products for these model catalysts. Probably, these differences should be associated with the control of the Ca/(P + Al) ratio for the catalysts. From XPS data, the atomic ratios were 0.05 for Ca/Al_2O_3, 0.17 for CaP/Al_2O_3, and 1.52 for HAP, although the XPS analysis showed that the surface Ca/P ratio of HAP was higher than the alumina-supported Ca/P ratios. For a relative lower molar ratio the catalyst acts as an acid catalyst (overall acidity order Ca/Al_2O_3 ≅ Ca-P/Al_2O_3 > HAP); however, with Ca/P ratio higher than 1.50 it means that the catalyst would also act as a basic catalyst, favoring in this way acetaldehyde formation by dehydrogenation (overall basicity order HAP > Ca/Al_2O_3 > Ca-P/Al_2O_3) involving mainly monodentate-species (CH_3CH_2O-Ca).

No DEE formation was detected for HAP in the whole temperature interval (in according to the abscense of bidentate ethoxy-species); however, Ca/Al_2O_3 produces DEE from 495 K with a maximum at 645 K. For Ca-P/Al_2O_3 catalyst this product was detected at 450 K, with a maxima at 571 K; 75° lower than Ca/Al_2O_3 catalyst, that can be correlated to bidentate species strength. The formation of DEE occurs by the dehydration of ethanol over acid sites associated with an uncovered alumina-support surface (γ-Al_2O_3) and, at a lower temperature, by the participation of Brönsted acid sites related to P centers (HPO_4^{2-}), as reported by Silvester *et al.*[28] A negligible contribution of ethylene was detected for HAP; meanwhile, Ca/Al_2O_3 and Ca-P/Al_2O_3 catalysts produced similar but a relatively low quantity of ethylene at 416 K, and a considerable contribution at higher temperatures, with maxima at 697 K and 751 K for Ca-P/Al_2O_3 and Ca/Al_2O_3 catalysts, respectively; i.e., 50° difference between the maximum and lower for the catalyst containing P, as was registered by FTIR spectra. It is recognized that the dehydration of alcohols essentially takes place on Brönsted acid sites whereas Lewis acid sites rarely contribute to this reaction. Besides, the formation of ethylene is dominated by high reaction temperatures because it is an endothermic reaction, whereas DEE mainly occurs at lower reaction temperatures due to its exothermic character.

The profile of *n*-butanol at different temperatures over different catalysts is also shown in the right upper panel of Fig. 6. It can be observed that HAP showed maximum production at 704 K and 60° above the maximum for the Ca/Al_2O_3 catalyst (T_{max} = 763 K). For P-containing catalysts (Ca-P/Al_2O_3) no butanol formation was detected; probably this lack of butanol production was associated with the fact that the ethanol is preferentially directed to DEE and ethylene production by the higher overall acidity of the system and by the lower basicity decreasing the interaction between acetaldehyde and the catalyst surface.[22] Acetaldehyde is formed in the low temperature range and is released in the gas phase due to a weak interaction with the catalyst surface, diminising, in part, its condensation route for *n*-butanol formation.

The performance described for HAP and Ca/Al_2O_3 is almost comparable since they showed similar basic sites distribution, although, they present some differences founded in the overall acidity of the catalysts registered by NH_3-TPD tests and they are active for ethanol transformation to butanol. However, Ca-P/Al_2O_3 catalyst is able to desorb ethanol and form acetaldehyde through ethoxide species at low temperatures, and so, this catalyst is able to convert ethanol into ethylene at temperatures higher than 700 K and DEE in the temperature interval between 550 and 650 K, respectively. This last can be attributed to combined P-species and Al_2O_3-support acidity centers resulting this catalyst almost inactive for *n*-butanol production.

Direct route for 1-butanol formation occurs by dimerization of two molecules of ethanol at low temperatures involving basic metal oxides.[14] The production of *n*-butanol, as Scalbert *et al.*[23] reported, also occurs by aldol condensation of two molecules of acetaldehyde at low temperatures in different steps. So, acetaldehyde is considered as an intermediate of reaction (indirect route), generated both by the non-oxidative dehydrogenation on basic-sites preferentially Ca-O-Ca centers[25] (present in alumina supported catalysts) and Ca-O-Ca-O-Al sites

or by the decomposition of surface ethoxide-species; considering that the amount of basic sites is enough to carry out the reaction, the differences in the product distribution would be associated with the presence of acid–base cooperative centers.[53] The formation of *n*-butanol would be promoted by those catalysts able to stabilize the adsorbed acetaldehyde and by self-condensation involving Ca-O-P and Ca-O-Al sites[26,28,54] to form acetaldol (3-hydrobutanal) or the carbanion formed upon ethanol adsorption on catalyst; however the aldol-condensation (ethanol and acetaldehyde) will promote the butene species that were not detected for these model catalysts and the stabilization of carbanion would favor ethylene and DEE production in acid sites. Besides, crotyl alcohol derives necessarily from crotonaldehyde formed by Meerwein–Ponndorf–Verley–Oppenhauer (MPVO) reduction reaction with ethanol as the reductant agent. Acetaldehyde was formed at the same time (as a second route) and is also detected at higher temperatures, and 1-butanol formed via crotyl alcohol reduction by ethanol, with a drop-signal by ethanol consumption, over Ca/Al_2O_3 and HAP catalysts can be evidenced.

Calcium-based bifunctional catalysts (HAP and Ca/Al_2O_3) are effective for butanol production from ethanol coupling; the catalysts are able to integrate multifunctional and accessible sites for these chemical routes: non-oxidative dehydrogenation, aldol condensation and intermolecular reduction by step processes, with a tuned balance of basic and acid sites. Biobutanol is a diesel substitute because is a non-polar alcohol with long hydrocarbon chains, which can be used as fuel directly or blended in existing thermal engines.

Conclusions

Calcium-based bifunctional acid-basic model catalysts for biobutanol production were prepared, characterized and tested in ethanol condensation reaction by 'under working' techniques. By the formulation of model catalysts, new insights have been gained that allow the mechanism of the chemical pathway by which *n*-biobutanol is produced to be identified through a bioethanol sustainable coupling process. Ca/Al_2O_3 and $Ca\text{-}P/Al_2O_3$, compared with the most butanol selective HAP catalyst, showed a different balance of basic and acid sites and therefore different catalytic activity. Three major steps have been identified for biobutanol production: non-oxidative dehydrogenation, aldol condensation, and intermolecular reduction, associated with basic-acid sites Ca-O-Ca/Ca-O-P/Ca-O-Al.

Acknowledgements

The authors would like to acknowledge the financial support of the CTQ 2017-87909R project. M.C.R. acknowledges the postdoctoral fellowship obtained from the University of Malaga.

References

1. Vojtisek-Lom M, Beránek V, Mikuška P, Křůmal K, Coufalík P, Sikorová J *et al.*, Blends of butanol and hydrotreated vegetable oils as drop-in replacement for diesel engines: Effects on combustion and emissions. *Fuel* **197**:407–421 (2017). https://doi.org/10.1016/j.fuel.2017.02.039.
2. Fagundez JLS, Golke D, Martins MES and Salau NPG, An investigation on performance and combustion characteristics of pure n-butanol and a blend of n-butanol/ethanol as fuels in a spark ignition engine. *Energy* **176**:521–530 (2019). https://doi.org/10.1016/j.energy.2019.04.010.
3. Gabriëls D, Hernández WY, Sels BF, Van Der Voort P and Verberckmoes A, Review of catalytic systems and thermodynamics for the Guerbet condensation reaction and challenges for biomass valorization. *Cat Sci Technol* **5**:3876–3902 (2015). https://doi.org/10.1039/c5cy00359h.
4. Galadima A and Muraza O, Catalytic upgrading of bioethanol to fuel grade Biobutanol: a review. *Ind Eng Chem Res* **54**:7181–7194 (2015). https://doi.org/10.1021/acs.iecr.5b01443.
5. Kozlowski JT and Davis RJ, Heterogeneous catalysts for the Guerbet coupling of alcohols. *ACS Catal.* **3**:1588–1600 (2013). https://doi.org/10.1021/cs400292f.
6. Wu X, Fang G, Tong Y, Jiang D, Liang Z, Leng W *et al.*, Catalytic upgrading of ethanol ton-butanol: progress in catalyst development. *ChemSusChem* **11**:71–85 (2018). https://doi.org/10.1002/cssc.201701590.
7. Aitchison H, Wingad RL and Wass DF, Homogeneous ethanol to butanol catalysis—Guerbet renewed. *ACS Catal* **6**:7125–7132 (2016). https://doi.org/10.1021/acscatal.6b01883.
8. Carvalho DL, De Avillez RR, Rodrigues MT, Borges LEP and Appel LG, Mg and Al mixed oxides and the synthesis of n-butanol from ethanol. *Appl Catal A Gen* **415–416**:96–100 (2012). https://doi.org/10.1016/j.apcata.2011.12.009.
9. Sun Z, Vasconcelos AC, Bottari G, Stuart MCA, Bonura G, Cannilla C *et al.*, Efficient catalytic conversion of ethanol to 1-butanol via the Guerbet reaction over copper- and nickel-doped porous. *ACS Sustain Chem Eng* **5**:1738–1746 (2017). https://doi.org/10.1021/acssuschemeng.6b02494.
10. Quesada J, Faba L, Díaz E and Ordóñez S, Enhancement of the 1-butanol productivity in the ethanol condensation catalyzed by noble metal nanoparticles supported on Mg-Al mixed oxide. *Appl Catal Gen* **563**:64–72 (2018). https://doi.org/10.1016/j.apcata.2018.06.037.
11. N. V. Vlasenko, P.I. Kyriienko, O.I. Yanushevska, K. V. Valihura, S.O. Soloviev, P.E. Strizhak, Catal Letters (2020). https://doi.org/10.1007/s10562-019-02937-x, 234, 242.
12. Benito P, Vaccari A, Antonetti C, Licursi D, Schiarioli N, Rodriguez-Castellón E *et al.*, Tunable copper-hydrotalcite derived mixed oxides for sustainable ethanol condensation to n-butanol in liquid phase. *J Clean Prod* **209**:1614–1623 (2019). https://doi.org/10.1016/j.jclepro.2018.11.150.
13. Yang C and Meng Z, Bimolecular condensation of ethanol to 1-butanol catalyzed by alkali cation zeolites. *J Catal* **142**:37–44 (1993). https://doi.org/10.1006/jcat.1993.1187.

14. Chieregato A, Ochoa JV, Bandinelli C, Fornasari G, Cavani F and Mella M, On the chemistry of ethanol on basic oxides: revising mechanisms and intermediates in the Lebedev and Guerbet reactions. *ChemSusChem* **8**:377–388 (2015). https://doi.org/10.1002/cssc.201402632.
15. Birky TW, Kozlowski JT and Davis RJ, Isotopic transient analysis of the ethanol coupling reaction over magnesia. *J Catal* **298**:130–137 (2013). https://doi.org/10.1016/j.jcat.2012.11.014.
16. León M, Díaz E, Vega A, Ordóñez S and Auroux A, Consequences of the iron–aluminium exchange on the performance of hydrotalcite-derived mixed oxides for ethanol condensation. *Appl Catal Environ* **102**:590–599 (2011). https://doi.org/10.1016/j.apcatb.2010.12.044.
17. Quesada J, Faba L, Díaz E and Ordóñez S, Role of the surface intermediates in the stability of basic mixed oxides as catalyst for ethanol condensation. *Appl Catal Gen* **542**:271–281 (2017). https://doi.org/10.1016/j.apcata.2017.06.001.
18. Quesada J, Faba L, Díaz E and Ordóñez S, Copper-basic sites synergic effect on the ethanol dehydrogenation and condensation reactions. *ChemCatChem* **10**:3583–3592 (2018). https://doi.org/10.1002/cctc.201800517.
19. Riittonen T, Toukoniitty E, Madnani DK, Leino A-R, Kordas K, Szabo M *et al*., One-pot liquid-phase catalytic conversion of ethanol to 1-butanol over aluminium oxide—the effect of the active metal on the selectivity. *Catalysts* **2**:68–84 (2012). https://doi.org/10.3390/catal2010068.
20. Riittonen T, Eränen K, Mäki-Arvela P, Shchukarev A, Rautio AR, Kordas K *et al*., Continuous liquid-phase valorization of bio-ethanol towards bio-butanol over metal modified alumina. *Renew Energy* **74**:369–378 (2014). https://doi.org/10.1016/j.renene.2014.08.052.
21. Rodrigues EG, Keller TC, Mitchell S and Pérez-Ramírez J, Hydroxyapatite, an exceptional catalyst for the gas-phase deoxygenation of bio-oil by aldol condensation. *Green Chem* **16**:4870–4874 (2014). https://doi.org/10.1039/c4gc01432d.
22. Hanspal S, Young ZD, Prillaman JT and Davis RJ, Influence of surface acid and base sites on the Guerbet coupling of ethanol to butanol over metal phosphate catalysts. *J Catal* **352**:182–190 (2017). https://doi.org/10.1016/j.jcat.2017.04.036.
23. Scalbert J, Thibault-Starzyk F, Jacquot R, Morvan D and Meunier F, Ethanol condensation to butanol at high temperatures over a basic heterogeneous catalyst: How relevant is acetaldehyde self-aldolization? *J Catal* **311**:28–32 (2014). https://doi.org/10.1016/j.jcat.2013.11.004.
24. Faria RMB, César DV and Salim VMM, Surface reactivity of zinc-modified hydroxyapatite. *Catal Today* **133–135**:168–173 (2008). https://doi.org/10.1016/j.cattod.2007.12.114.
25. Ben Osman M, Krafft J-M, Thomas C, Yoshioka T, Kubo J and Costentin G, Importance of the nature of the active acid/base pairs of hydroxyapatite involved in the catalytic transformation of ethanol to n-butanol revealed by operando DRIFTS. *ChemCatChem* **11**:1765–1778 (2019). https://doi.org/cctc.10.1002/201801880.
26. Ho CR, Shylesh S and Bell AT, Mechanism and kinetics of ethanol coupling to butanol over hydroxyapatite. *ACS Catal.* **6**:939–948 (2016). https://doi.org/10.1021/acscatal.5b02672.
27. Tsuchida T, Kubo J, Yoshioka T, Sakuma S, Takeguchi T and Ueda W, Reaction of ethanol over hydroxyapatite affected by Ca/P ratio of catalyst. *J Catal* **259**:183–189 (2008). https://doi.org/10.1016/j.jcat.2008.08.005.
28. Silvester L, Lamonier J-F, Faye J, Capron M, Vannier R-N, Lamonier C *et al*., Reactivity of ethanol over hydroxyapatite-based Ca-enriched catalysts with various carbonate contents. *Cat Sci Technol* **5**:2994–3006 (2015). https://doi.org/10.1039/C5CY00327J.
29. Ogo S, Onda A, Iwasa Y, Hara K, Fukuoka A and Yanagisawa K, 1-Butanol synthesis from ethanol over strontium phosphate hydroxyapatite catalysts with various Sr/P ratios. *J Catal* **296**:24–30 (2012). https://doi.org/10.1016/j.jcat.2012.08.019.
30. Silvester L, Lamonier JF, Lamonier C, Capron M, Vannier RN, Mamede AS *et al*., Guerbet reaction over strontium-substituted hydroxyapatite catalysts prepared at various (Ca+Sr)/P ratios. *ChemCatChem* **9**:2250–2261 (2017). https://doi.org/10.1002/cctc.201601480.
31. Pang J, Zheng M, He L, Li L, Pan X, Wang A *et al*., Upgrading ethanol to n-butanol over highly dispersed Ni–MgAlO catalysts. *J Catal* **344**:184–193 (2016). https://doi.org/10.1016/j.jcat.2016.08.024.
32. Sun J and Wang Y, Recent advances in catalytic conversion of ethanol to chemicals. *ACS Catal.* **4**:1078–1090 (2014). https://doi.org/10.1021/cs4011343.
33. Kozlowski JT, Davis RJ and Energy J, Sodium modification of zirconia catalysts for ethanol coupling to 1-butanol. *Chem* **22**:58–64 (2013). https://doi.org/10.1016/S2095-4956(13)60007-8.
34. Ndou AS, Plint N and Coville NJ, Dimerisation of ethanol to butanol over solid-base catalysts. *Appl Catal Gen* **251**:337–345 (2003). https://doi.org/10.1016/S0926-860X(03)00363-6.
35. Gines MJL and Iglesia E, Bifunctional condensation reactions of alcohols on basic oxides modified by copper and potassium. *J Catal* **176**:155–172 (1998). https://doi.org/10.1006/jcat.1998.2009.
36. Liu YY, Qin GH, Song XY, Ding JW, Liu FS, Yu ST *et al*., Mesoporous alumina modified calcium catalyst for alcoholysis of polycarbonate. *Chem Eng* **86**:222–229 (2018). https://doi.org/10.1016/j.jtice.2018.02.028.
37. Chung RJ, Hsieh MF, Panda RN and Chin TS, Hydroxyapatite layers deposited from aqueous solutions on hydrophilic silicon substrate. *Surf Coatings Technol* **165**:194–200 (2003). https://doi.org/10.1016/S0257-8972(02)00731-4.
38. Demri B and Muster D, XPS study of some calcium compounds. *J Mater Process Technol* **55**:311–314 (1995). https://doi.org/10.1016/0924-0136(95)02023-3.
39. Silvester L, Lamonier JF, Vannier RN, Lamonier C, Capron M, Mamede AS *et al*., Structural, textural and acid–base properties of carbonate-containing hydroxyapatites. *J Mater Chem A* **2**:11073–11090 (2014). https://doi.org/10.1039/c4ta01628a.
40. Phung TK, Herrera C, Larrubia MÁ, García-Diéguez M, Finocchio E, Alemany LJ *et al*., Surface and catalytic properties of some γ-Al2O3 powders. *Appl Catal Gen* **483**:41–51 (2014). https://doi.org/10.1016/j.apcata.2014.06.020.
41. Diallo-Garcia S, Ben Osman M, Krafft J-M, Casale S, Thomas C, Kubo J *et al*., Identification of surface basic sites and acid–base pairs of hydroxyapatite. *J Phys Chem C* **118**:12744–12757 (2014). https://doi.org/10.1021/jp500469x.
42. Perrone OM, Lobefaro F, Aresta M, Nocito F, Boscolo M and Dibenedetto A, Butanol synthesis from ethanol over CuMgAl mixed oxides modified with palladium (II) and indium (III). *Fuel Process Technol* **177**:353–357 (2018). https://doi.org/10.1016/j.fuproc.2018.05.006.
43. Petrolini DD, Eagan N, Ball MR, Burt SP, Hermans I, Huber GW *et al*., Ethanol condensation at elevated pressure over copper on AlMgO and AlCaO porous mixed-oxide supports. *Cat Sci Technol* **9**:2032–2042 (2019). https://doi.org/10.1039/c9cy00316a.

44. Hun J, Lee J, Szanyi J and Peden CHF, Modification of the acid/base properties of γ-Al2O3 by oxide additives: An ethanol TPD investigation. *Catal. Today* **265**:240–244 (2016). https://doi.org/10.1016/j.cattod.2015.07.042.
45. Resini C, Cavallaro S, Frusteri F, Freni S and Busca G, Initial steps in the production of H2 from ethanol: A FT-IR study of adsorbed species on Ni/MgO catalyst surface. *React Kinet Catal Lett* **90**:117–126 (2007). https://doi.org/10.1007/s11144-007-5027-2.
46. Dömök M, Tóth M, Raskó J and Erdohelyi A, Adsorption and reactions of ethanol and ethanol–water mixture on alumina-supported Pt catalysts. *Appl Catal Environ* **69**:262–272 (2007). https://doi.org/10.1016/j.apcatb.2006.06.001.
47. Carvalho DL, Borges LEP, Appel LG, Ramírez De La Piscina P and Homs N, In situ infrared spectroscopic study of the reaction pathway of the direct synthesis of n-butanol from ethanol over MgAl mixed-oxide catalysts. *Catal Today* **213**:115–121 (2013). https://doi.org/10.1016/j.cattod.2013.03.034.
48. Young ZD, Hanspal S and Davis RJ, Aldol condensation of acetaldehyde over titania, hydroxyapatite, and magnesia. *ACS Catal.* **6**:3193–3202 (2016). https://doi.org/10.1021/acscatal.6b00264.
49. Garbarino G, Wang C, Valsamakis I, Chitsazan S, Riani P, Finocchio E *et al*., Acido-basicity of lanthana/alumina catalysts and their activity in ethanol conversion. *Appl Catal Environ* **200**:458–468 (2017). https://doi.org/10.1016/j.apcatb.2016.07.010.
50. Phung TK and Busca G, Diethyl ether cracking and ethanol dehydration: Acid catalysis and reaction paths. *Chem Eng J* **272**:92–101 (2015). https://doi.org/10.1016/j.cej.2015.03.008.
51. Nair H, Gatt JE, Miller JT and Baertsch CD, Mechanistic insights into the formation of acetaldehyde and diethyl ether from ethanol over supported VOx, MoOx, and WOx catalysts. *J Catal* **279**:144–154 (2011). https://doi.org/10.1016/j.jcat.2011.01.011.
52. Oyama ST and Zhang W, True and spectator intermediates in catalysis: The case of ethanol oxidation on molybdenum oxide as observed by in situ laser Raman spectroscopy. *J Am Chem Soc* **118**:7173–7177 (1996). https://doi.org/10.1021/ja960468v.
53. Larina OV, Valihura KV, Kyriienko PI, Vlasenko NV, Balakin DY, Khalakhan I *et al*., Successive vapour phase Guerbet condensation of ethanol and 1-butanol over Mg-Al oxide catalysts in a flow reactor. *Appl Catal Gen* **588**:117265 (2019). https://doi.org/10.1016/j.apcata.2019.117265.
54. Di Cosimo JI, Apesteguía CR, Ginés MJL and Iglesia E, Structural requirements and reaction pathways in condensation reactions of alcohols on MgyAlOx catalysts. *J Catal* **190**:261–275 (2000). https://doi.org/10.1006/jcat.1999.2734.

Marina Pinzón

Marina Pinzón obtained her degree and her MsC in Chemical Engineering in 2016 at 2018, respectively, from the University of Málaga. She worked as a collaborator with the PROCAT group of the Chemical Engineering Department. Currently, she is a predoctoral researcher at UCLM, working on finding catalysts for ammonia decomposition reaction to produce hydrogen.

Marina Cortés-Reyes

Dr Marina Cortés-Reyes is a lecturer in the Chemical Engineering Department at the University of Malaga. She received her PhD degree in chemical engineering, and her MSc in advanced chemistry, and the preparation and characterization of materials, from the University of Malaga. Her work focuses on the synthesis, characterization, and activity analysis of heterogeneous catalysts for environmental and energy applications.

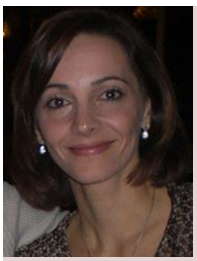

Concepción Herrera

Dr Concepción Herrera is associate professor in the Chemical Engineering Department at the University of Malaga. She works in the area of chemical technology, focusing on the development of catalytic strategies with application to processes of interest, mainly aimed at the production of bio-fuels, as well as in the NOx and soot abatement. She has participated in different research projects on these topics. She is currently the head of the Chemical Engineering Department of the University of Málaga.

Maria Á. Larrubia

Dr M. Ángeles Larrubia is full professor of chemical engineering and vice-dean of the Faculty of Sciences of the University of Malaga. Her research focuses on the study of the catalytic properties of different materials with different applications. She has around 80 scientific publications and has participated in different national and European projects.

Luis J. Alemany

Dr Luis J. Alemany is full professor of chemical engineering, head of the PROCAT research group, and coordinator of chemical engineering master at the University of Malaga. His research is focused on the catalytic process technologies for energy and environmental applications. He has been the principal researcher in contract and research projects with a hundred publications in the field of chemical engineering.

